

Supporting Information

**Co-biomembrane coated Fe₃O₄/MnO₂ multifunctional nanoparticles for targeted delivery
and enhanced chemodynamic/photothermal/chemo therapy**

Yingshu Guo,^{*a,b} Xiaofei Zheng,^b Tingting Gai,^a Zhiyong Wei^c and Shusheng Zhang^{*b}

^a Shandong Provincial Key Laboratory of Molecular Engineering, School of Chemistry and Chemical Engineering, Qilu University of Technology (Shandong Academy of Sciences), Jinan 250353, China.

^b School of Chemistry and Chemical Engineering, Linyi University, Linyi 276005, China.

^c Linyi people's hospital, Linyi 276005, China.

*Corresponding email address: yingshug@126.com; shushzhang@126.com

EXPERIMENTAL SECTION

Materials

NH₂-Fe₃O₄ magnetic nanospheres were purchased from Tianjin BaseLine Chromatographic Technology Development Center. And 3,3',5,5'-tetramethylbenzidine (TMB), N-(3-Dimethylaminopropyl)-N-ethylcarbodiimide hydrochloride (EDC) and N-Hydroxysuccinimide (NHS) were purchased from Shanghai Aladdin Biochemical Technology Co., Ltd. Bovine serum albumin (BSA) and Doxorubicin hydrochloride (DOX) were provided by Sangon Biotech (Shanghai) Co., Ltd. *Escherichia coli* MG1655 was purchased from Shanghai Xinyu Biotechnology Co., Ltd. LB broth medium was purchased from Beijing Luqiao Technology Co., Ltd. Agar Powder, Hoechst33342, 3-[4,5-Dimethylthiazol-2-yl]-2,5-diphenyltetrazolium-biomide (MTT) were provided by Beijing Solarbia Technology Co., Ltd. MCF-7 cells (human breast cancer cells from Michigan Cancer Foundation) and L02 cells (human embryonic liver cells) were purchased from Procell Life Science & Technology Co., Ltd. Dulbeccos Modified Eagle Medium(DMEM), Fetal Bovine Serum (FBS) and Trypsin were provided by Invitgen (USA). PAH, MES were provided by Shanghai Macklin biochemical Technology Co., Ltd. KMnO₄ was purchased from the Fine Chemical Plant of Laiyang Economic and technological Development Zone (China). All other reagents were analytical pure reagents, which can be directly used without further purification. All the water used in the experiment was sterilized ultra-pure water. All glassware was cleaned with fresh aqua regia (HCl/HNO₃=3:1, v/v) before use. All animal experimental procedures and techniques were approved by the Animal Ethics Committee of Linyi University, and methods were carried out in accordance with the approved guidelines and laws.

Apparatus

Absorption spectra were determined by a UV–vis spectrophotometer (Cary 60, Agilent). Size and Zeta potential measurement was performed at 25°C on a Zeta-Size Nano instrument (Zen 3600, Malvern Instruments Ltd.). Transmission electron microscope images (TEM) were performed transmission electron microscope (JEM-2100, JEOL). Confocal fluorescence imaging was performed on a confocal laser scanning microscope (LEICA TCS SP8, Germany).

Principle of the Strategy

MnO₂ NPs were synthesized by a one-step reduction method. At the same time, composite nanoparticles were obtained by coupling MnO₂ NPs with NH₂-Fe₃O₄. NDH-2 in the EM can accept electrons from NADH and then transfer electrons to oxygen to produce H₂O₂. Therefore, the EM was loaded onto composite nanoparticles to compensate for the deficiency of endogenous H₂O₂ in tumor cells. Fenton-like reaction can occur between Fe₃O₄/MnO₂ and H₂O₂ to produce •OH, which has a certain degree of toxicity to tumor cells. At the same time, because of its excellent photothermal properties, Fe₃O₄/MnO₂ can generate more heat under 808nm laser irradiation, which can be used in the cooperative treatment of tumors. At the same time, Fe₃O₄/MnO₂/MM/EM/D can achieve the targeted delivery of DOX, thereby reducing damage to normal cells. Of course, to enhance the targeting ability of nano-drugs, we loaded MM onto the nanoparticles to achieve homologous targeting of tumor cells.

Preparation of Fe₃O₄/MnO₂ NPs

We used one-step reduction method, that is, directly mix KMnO₄ (aq) and PAH (aq) to prepare MnO₂ NPs. In other words, 3 mL 37.4 mg mL⁻¹ PAH (aq) was first added to 20 mL 3.5 mg mL⁻¹ KMnO₄ (aq) drop by drop and stirred fully for 25 minutes at room temperature to get a brown solution. The obtained solution was mixed with deionized water, centrifuged under 14800 r

min⁻¹ for 20 min, ultrasonic at 70 W for 5 min, and washed for three times to obtain pure and stable MnO₂ NPs. To prepare BSA coated MnO₂, 0.05 g BSA was added to 2 mL MnO₂ NPs in a certain proportion. Then 0.018 g NaCl was added to make the solution into 0.9% normal saline, which was fully mixed to obtain BSA modified MnO₂ (BSA/MnO₂). 500 μL BSA/MnO₂ was taken into the 2 mL centrifuge tube, and 200 μL 20 mM EDC solution (10 mM pH=5.5 MES buffer solution) and 200 μL 35 mM NHS solution (10 mM pH=5.5 MES buffer solution) were added to the centrifuge tube, and the 30 min was mixed by shaking at 37°C. After the activation was completed, 400 μL NH₂-Fe₃O₄ NPs with the mass concentration of 2 mg mL⁻¹ after pH=7.0 Tris-HCl washing were added to the mixed solution, and the Fe₃O₄/MnO₂ NPs were obtained by shaking at 37°C for 12 hours.

Preparation of Fe₃O₄/MnO₂/MM/EM/D NPs

MCF-7 cells were treated by ultrasonic cell crusher (120 W, with an interval of 5 s) under the condition of ice bath for 20 minutes, to obtain the cell fragmentation solution. Then 10 min was centrifuged at 4°C and 500×g to remove cell contents, and then the supernatant was centrifuged at 10000×g for 10 min and 100000×g for 1 h to obtain MCF-7 breast cancer cell membrane. A similar method was used to deal with *Escherichia coli* and extract *Escherichia coli* membrane. 400 μL MCF-7 cell membrane and *Escherichia coli* membrane were respectively added to the 5 mL centrifuge tube, and 200 μL EDC and NHS solutions were added at the same time to shake at 25°C for 30 minutes. After the reaction was completed, 500 μL Fe₃O₄/MnO₂ was added into the shaker to shake for 8 hours at 25°C, and the dispersion of nanoparticles modified by composite membrane was obtained. The nano-particle dispersion modified by the composite membrane was washed for three times by magnetic force frame, and the washed product was dispersed in 1mL

PBS. The DOX solution of 20 μL 25 mg mL^{-1} was added and fully mixed for 24 hours. The solution after reaction was washed by magnetic force frame, and $\text{Fe}_3\text{O}_4/\text{MnO}_2/\text{MM}/\text{EM}/\text{D}$ was obtained.

Cell culture

MCF-7 cells and L02 cells were cultured with Dulbecco's Modified Eagle Medium (containing 10% FBS and 1% double antibiotics) in a 37°C constant temperature and humidity incubator with 5% CO_2 concentration.

Photothermal efficiency test of materials

$\text{Fe}_3\text{O}_4/\text{MnO}_2$, $\text{Fe}_3\text{O}_4/\text{MnO}_2/\text{MM}/\text{EM}/\text{D}$ and PBS were irradiated by 808 nm laser with the power of 3.52 W cm^{-2} (the energy density of 1056 J cm^{-2}) for 5 minutes respectively. The infrared thermal imager was used to collect the images at different time points, and the data processing system was used to get the temperature change curves of different time periods.

Cellular uptakes

1×10^5 MCF-7 cells and L02 cells were cultured in small dishes, incubated in an incubator for 12 hours, and incubated with $\text{Fe}_3\text{O}_4/\text{MnO}_2/\text{MM}/\text{EM}/\text{D}$ for 12 hours. Then the suspension cells were obtained by trypsin digestion, the cells were washed thoroughly with PBS, and the content of elements in the cells was determined by ICP-OES.

MTT assay

The cytotoxicity of nanoparticles to the cells was assessed by MTT analysis. MCF-7 cells were inoculated into 96-well plates with a cell density of about 10000 cells per well. After the 96-well plates were incubated at 37°C for 24 hours, the cells were incubated with nanoparticles for 3 h, 6 h, 9 h, 12 h, and 24 h. Then carefully remove the supernatant, add 100 μL of fresh culture

medium (containing 10% MTT solution) and continue to incubation for 4 hours. Remove the supernatant from the well plate and add 100 μ L DMSO to each well. Then shake at a low speed on the oscillator for ten minutes to completely dissolve the formazan crystals. Finally, the absorbance of each well was measured at 490 nm.

Cell internalization experiment

In order to study the intracellular uptake of nanoparticles, MCF-7 cells and L02 cells cultured in confocal petri dishes were stained with Hoechst33342 for 15 minutes and then washed with PBS for three times. The $\text{Fe}_3\text{O}_4/\text{MnO}_2/\text{MM}/\text{EM}/\text{D}$ were then added to the cells and incubated for 4 hours. After incubation, the cells were washed thoroughly with PBS, and then the intracellular internalization of the nanoparticles was detected by confocal microscope.

In vivo temperature measurement

In order to verify the photothermal conversion efficiency in vivo, 100 μ L MCF-7 cells were subcutaneously injected into female mice to establish a breast cancer model. Two weeks later, the tumor model was established successfully. 100 μ L PBS, $\text{Fe}_3\text{O}_4/\text{MnO}_2/\text{MM}/\text{EM}/\text{D}$ was injected into tumor-bearing mice through tail vein. After 12 hours of injection, the mice were anesthetized, and then the tumor was irradiated with 808 nm laser for 5 minutes at the power of 2.5 W cm^{-2} . Then the infrared thermal imager was used to measure the thermal image, and the accompanying software was used to record the photothermal temperature at different time points.

In Vivo Antitumor Efficacy

Anti-tumor experiment in vivo: the model of breast tumor was established by in situ injection of MCF-7 cells in mice. About a week after injection, when the tumor volume increased to about 100-150 mm^3 , the mice were randomly divided into four groups (nude 5). Two groups of tumor-

bearing mice were intravenously injected with PBS, and the other two groups of tumor-bearing mice were intravenously injected with Fe₃O₄/MnO₂/MM/EM/D. A group of mice in the PBS control group and the Fe₃O₄/MnO₂/MM/EM/D treatment group were irradiated with 808nm NIR laser under 2.5 W cm⁻² every two days. The body weight and tumor volume of tumor-bearing mice were measured every two days until the end of the experiment. The following formula was used to calculate the tumor volume (V): $V = (L \times W \times W) / 2$ (L: the maximum tumor diameter, W: the minimum diameter perpendicular to the length). After the end of the treatment cycle, the experimental mice were euthanized and the tumor tissues of each group were obtained. It was stored in tissue fixation solution to facilitate the post-production of paraffin sections and hematoxylin-eosin(H&E) staining analysis, so as to evaluate the effectiveness of various treatment methods.

Biosafety evaluation of composite nano-drugs: in order to evaluate the biosafety of Fe₃O₄/MnO₂/MM/EM/D, we injected PBS and Fe₃O₄/MnO₂/MM/EM/D intravenously into female non-tumor-bearing mice and tumor-bearing mice, respectively. At the same time, the tumor-bearing mice were irradiated by 808 nm laser with the power density of 2.5 W cm⁻². After 3 weeks of treatment, the mice were killed, and the hearts, livers, lungs and kidneys of the control group and the treatment group were collected. Then hematoxylin-eosin(H&E) analysis were used to evaluate the histopathological toxicity of typical tissues.

In order to optimize the preparation process of nanoparticles, we at various molar ratios between PAH and MnO_2 prepared MnO_2 , and measured the UV-visible absorption spectra of products prepared at different ratios. After reacting with PAH in a ratio of 2:1 and 3:1, the KMnO_4 peaks (315, 525, and 545 nm) disappeared. These samples showed a new broad peak near 300 nm, which indicates the formation of MnO_2 nanoparticles (Fig. S1A). During the synthesis process, the reduction of the amount of PAH is very important for in vivo applications, because the cationic polyelectrolyte may exhibit obvious concentration-dependent cytotoxicity. Based on this, when synthesizing MnO_2 , we reduced the amount of PAH to 3:1, as shown by the UV-vis spectra of samples prepared with different ratios of polyelectrolytes. At the same time, the influence of the ratio of various BSA/ MnO_2 on the zeta potential was explored. As $W_{\text{BSA}}/W_{\text{MnO}_2}$ gradually increased from 0 to 2.5%, its zeta potential was reduced from +28 mV to -25 mV, and continued to increase the amount of BSA, the potential change was not obvious, so we determined that $W_{\text{BSA}}/W_{\text{MnO}_2}=2.5\%$ is the best ratio for preparing BSA/ MnO_2 (Fig. S1B).

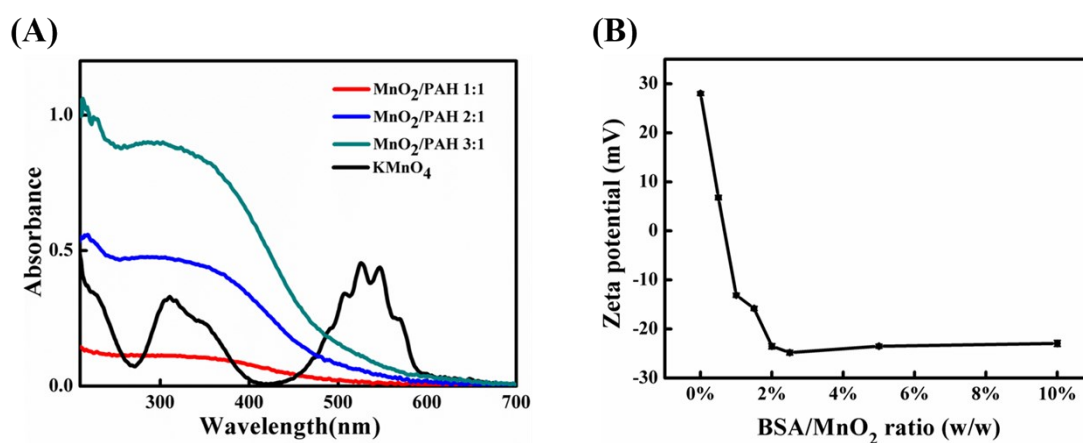


Fig. S1 (A) UV-vis absorption spectra of KMnO_4 solution and MnO_2 NPs prepared at various molar ratios between PAH and MnO_2 . (B) Effect of coating of MnO_2 with BSA on zeta potential for various BSA/ MnO_2 ratios.

The synthesis technology of $\text{NH}_2\text{-Fe}_3\text{O}_4$ is relatively developed and the purchased $\text{NH}_2\text{-Fe}_3\text{O}_4$

NPs have been previously characterized. First, $\text{NH}_2\text{-Fe}_3\text{O}_4$ NPs were characterized by transmission electron microscopy (TEM) and dynamic light scattering (DLS). Through TEM analysis, the Fe_3O_4 NPs without any coating and drug loading are approximately spherical. The average particle size was approximately 120 nm (Fig. S2A), and the diameter was approximately 140 nm in DLS (Fig. S2D). These results indicated that $\text{NH}_2\text{-Fe}_3\text{O}_4$ NPs have good dispersion in an aqueous solution. At the same time, the synthesized MnO_2 NPs were characterized. The representative TEM images showed that the average size of MnO_2 NPs was approximately 20 nm (Fig. S2B), and the diameter was approximately 25 nm in DLS (Fig. S2E). The polyelectrolyte used here can be used not only as a reducing agent to reduce KMnO_4 to MnO_2 , but also as a protective layer to stabilize nanoparticles due to electrostatic repulsion (zeta potential, + 27.96 mV, Fig. S2G). The zeta potential of BSA/MnO_2 was -24.32 mV (Fig. S2G). This value is close to the potential of BSA, which proves that BSA was successfully coated on the surface of the MnO_2 NPs. The representative TEM images showed that the average size of $\text{Fe}_3\text{O}_4/\text{MnO}_2/\text{MM}/\text{EM}/\text{D}$ was approximately 180 nm (Fig. S2C), and the hydrodynamic diameter was 200 nm (Fig. S2F). From the TEM image, it can be clearly seen that the composite nanoparticles were coated with a film-like substance, indicating that we successfully coated MM/EM to prepare $\text{Fe}_3\text{O}_4/\text{MnO}_2/\text{MM}/\text{EM}/\text{D}$. Similarly, the change in the zeta potential and the EDS analysis data also demonstrated the successful preparation of $\text{Fe}_3\text{O}_4/\text{MnO}_2/\text{MM}/\text{EM}/\text{D}$ (Fig. S2H-J).

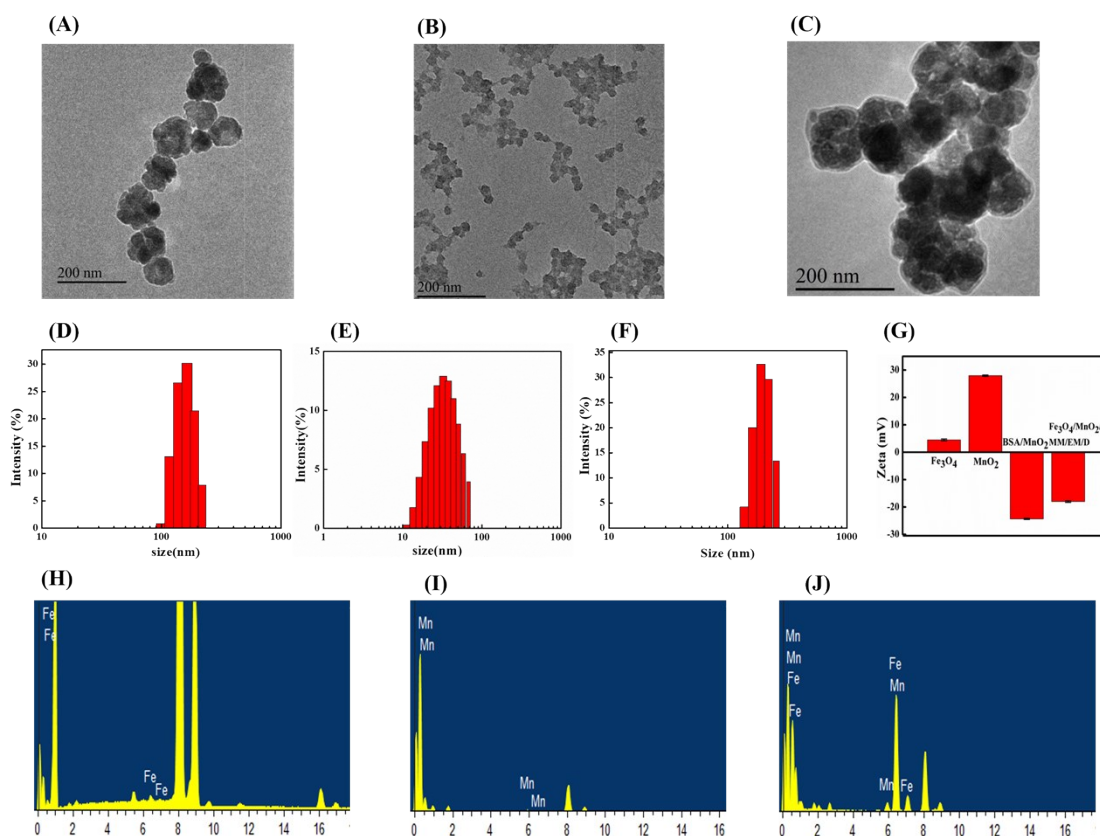


Fig. S2 (A) (B) (C) TEM images of Fe₃O₄, MnO₂ and Fe₃O₄/MnO₂/MM/EM/D. (D) (E) (F) Particle size of the Fe₃O₄, MnO₂ and Fe₃O₄/MnO₂/MM/EM/D. (G) Particle zeta potential of the Fe₃O₄, MnO₂, BSA/MnO₂ and Fe₃O₄/MnO₂/MM/EM/D. (H) (I) (J) EDS analysis of Fe₃O₄, MnO₂ and Fe₃O₄/MnO₂/MM/EM/D.

At the same time, UV-vis analysis proved the successful preparation of MnO₂ and BSA/MnO₂ (Fig. S3A). Compared with KMnO₄, the characteristic peaks at 315, 525 and 545 nm disappeared, and a new broad peak appeared near 300 nm, which is the characteristic peak of MnO₂ NPs. After the reaction with BSA, there is a characteristic absorption peak at 278 nm, which proves the successful preparation of BSA/MnO₂. As shown in Fig. S3B, Fe₃O₄/MnO₂ has the characteristic absorption peak of Fe₃O₄ and BSA/MnO₂ at the same time. This proves that Fe₃O₄/MnO₂ multifunctional composite nanoparticles were successfully synthesized. At the same time, the fluorescence signal of DOX was detected in Fe₃O₄/MnO₂/MM/EM/D, while the

fluorescence signal of DOX was not detected in Fe₃O₄/MnO₂/MM/EM, indicating that the nanoparticles successfully realized the loading of DOX (Fig. S3C).

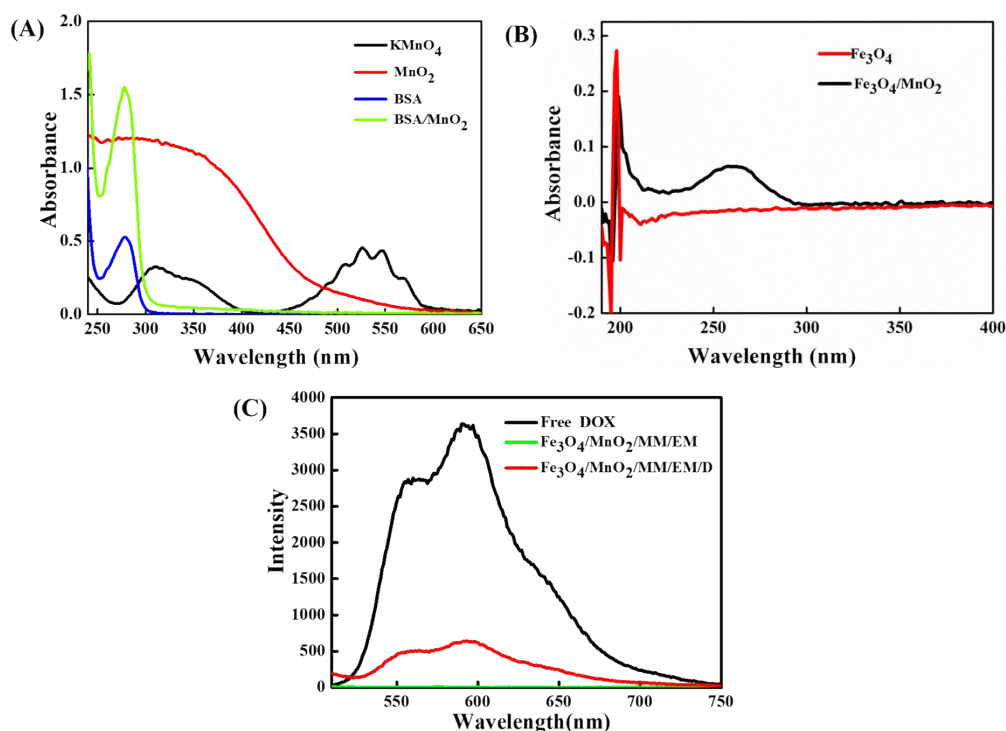


Fig. S3 (A)UV–vis absorption spectra of KMnO₄, MnO₂, BSA, and BSA/MnO₂ aqueous solution. (B)UV–vis absorption spectra of Fe₃O₄ and Fe₃O₄/MnO₂. (C)Fluorescence spectra of free DOX, Fe₃O₄/MnO₂/MM/EM and Fe₃O₄/MnO₂/MM/EM/D. The two samples had the same DOX concentration.

In the presence of NDH-2, a large amount of NADH is converted to NAD⁺. In this process, it is accompanied by the conversion of MTT to MTT-Formazan^{1,2}. Therefore, we designed to prove the existence of NDH-2 by monitoring the process of MTT conversion to MTT-Formazan (Fig. S4A). We measured the UV-visible absorption spectra of MTT, NADH, MTT/NADH, as well as MTT/NADH/EM after incubating 10 min at 25°C. Obviously, a higher absorbance was observed in the 300–460 nm range, and the maximum absorbance peak of MTT, NADH, MTT/NADH was 375,340 and 340 nm (the curves a, b and c), which are the characteristic absorption peaks of MTT

and NADH, respectively. The MTT/NADH/EM has higher absorbance in the range of 460~680 nm, and the maximum absorbance peaks are at 530 nm and 340 nm, respectively, indicating that MTT-Formazan has been formed (the curve d). In addition, the absorbance of the MTT/NADH/EM at 375 nm, that is, the characteristic absorption peak of MTT, is much lower than that of MTT solution (Fig. S4B). This indicated that the concentration of MTT decreased due to the conversion to MTT-Formazan. The color of the MTT/NADH/EM changes from colorless to dark purple, which clearly showed the formation of MTT-Formazan (Fig. S4B illustration). To sum up, it can be proved that EM contains NDH-2, and can catalyze the conversion of MTT to MTT-Formazan.

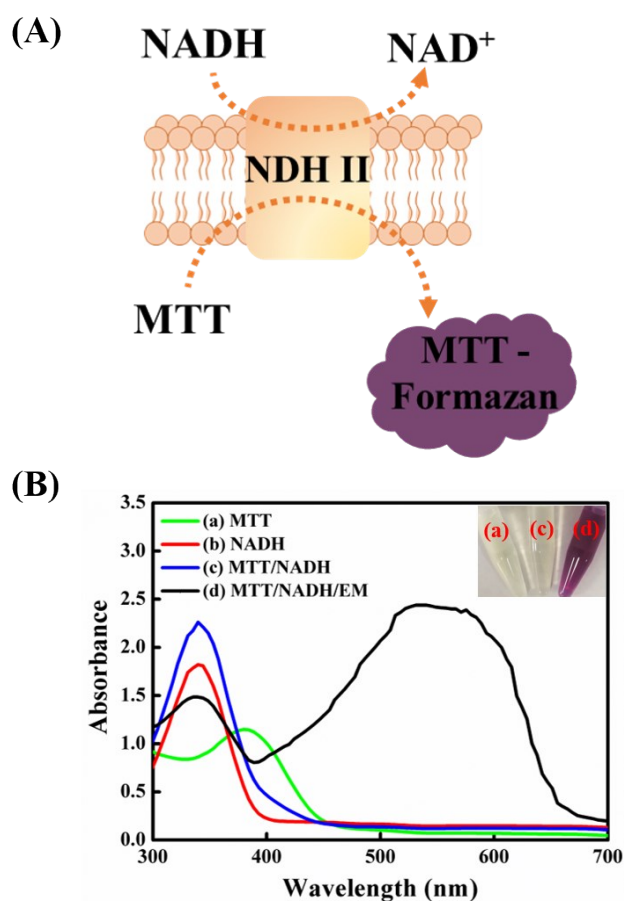


Fig. S4 (A) Schematic diagram of the formation of MTT-formazan catalyzed by NDH-2 based on *E. coli* membranes. (B) Absorbance spectra of (a) 0.5 mM MTT; (b) 1.0 mM NADH; (c) 0.5 mM

MTT and 1.0 mM NADH; and (d) 0.5 mM MTT, 1.0 mM NADH, and EM, after incubation for 10 min at 25°C.

We evaluated the ability of Fe₃O₄/MnO₂ to produce •OH under acidic conditions. First, the ability of Fe₃O₄/MnO₂ and H₂O₂ to form •OH by a Fenton-like reaction was determined by the 3,3',5,5'-tetramethylbenzidine (TMB) method. The essential discoloration principle of TMB reacting with H₂O₂ is TMB oxidized by the hydroxyl radical (•OH) and losing electron(s) to form colored oxidation products (oxTMB).³⁻⁵ TMB can be oxidized to become a turquoise color by highly active •OH, and the maximum absorption wavelength is approximately 650 nm. As shown in the Fig. S5A, even if the incubation time is prolonged, there was no obvious color change in the TMB aqueous solution of Fe₃O₄, MnO₂ and H₂O₂, and there was no obvious effect on the increase in the absorbance of TMB. In contrast, Fe₃O₄/MnO₂+H₂O₂ caused the color of the TMB aqueous solution to change to turquoise, and the absorbance of TMB was higher than that of Fe₃O₄ or MnO₂ and H₂O₂ alone, which proves that Fe₃O₄/MnO₂ can cooperatively catalyze the Fenton-like reaction to produce •OH effectively. At the same time, we found that Fe₃O₄/MnO₂ NPs can cause an obvious color change in TMB under weakly acidic conditions (pH=5.5) but not under neutral conditions (pH=7.4), and the trends of the absorbance of TMB is the same (Fig. S5B). The main reason is that Fe₃O₄/MnO₂ NPs can be dissociated into Fe²⁺/Mn²⁺ under acidic conditions to catalyze the Fenton-like reaction to produce •OH. These results show that Fe₃O₄/MnO₂ composite nanoparticles can efficiently catalyze the Fenton-like reaction to form •OH, which is expected to improve the therapeutic efficiency of CDT on tumors.

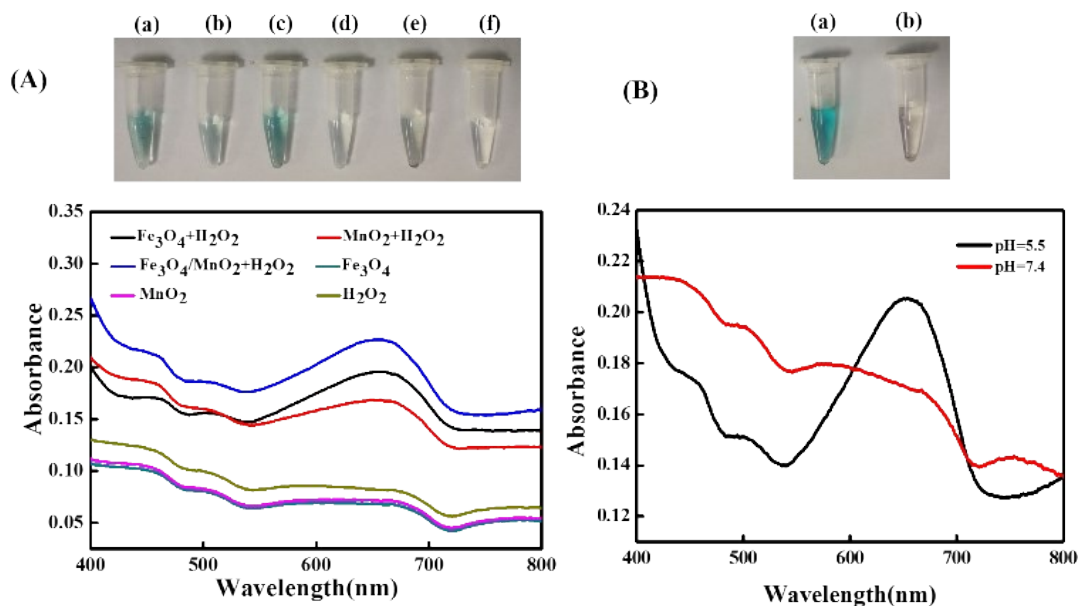


Fig. S5 (A) UV-vis spectra and photographs(inset) of TMB aqueous solution treated with (a) Fe₃O₄ + H₂O₂ (b) MnO₂+H₂O₂ (c) Fe₃O₄/MnO₂ + H₂O₂ (d) H₂O₂ (e) Fe₃O₄ (f) MnO₂. (B) UV-vis spectra and photographs(inset) of •OH generated by Fe₃O₄ /MnO₂ at different pH values (a) pH=5.5 (b) pH=7.4 based on TMB assay.

To characterize the photothermal effect of Fe₃O₄/MnO₂/MM/EM/D, we first verified the photothermal conversion effect in vitro. Through the experimental results, we can see that the temperatures of Fe₃O₄/MnO₂ NPs and Fe₃O₄/MnO₂/MM/EM/D were significantly increased by 808 nm NIR irradiation, indicating that the composite nanomaterials coated with the MM/EM still have high photothermal conversion properties. The coating of the membrane has little effect on the photothermal effect of the material itself. Under irradiation with an 808 nm NIR laser with a power density of 3.52 W cm⁻², the temperature of Fe₃O₄/MnO₂/MM/EM/D increased rapidly, and the temperature increased to approximately 49°C at 5 min and tended to stabilize gradually. At the same time, after irradiating Fe₃O₄/MnO₂ NPs with the same power density for 5 minutes, the temperature of Fe₃O₄/MnO₂ NPs increased to 51°C (Fig. S6A). In summary, the temperature of Fe₃O₄/MnO₂ NPs and Fe₃O₄/MnO₂/MM/EM/D increased by approximately 23°C after 6 min of

irradiation with an 808 nm NIR laser with a power density of 3.52 W cm^{-2} . However, after the same light treatment, the temperature of the phosphate-buffered saline (PBS) group increased by only approximately 3°C (Fig. S6B). The results showed that $\text{Fe}_3\text{O}_4/\text{MnO}_2/\text{MM}/\text{EM}/\text{D}$ have obvious photothermal conversion efficiency, so they can be used as a photothermal reagent to treat tumors by generating local high temperatures.

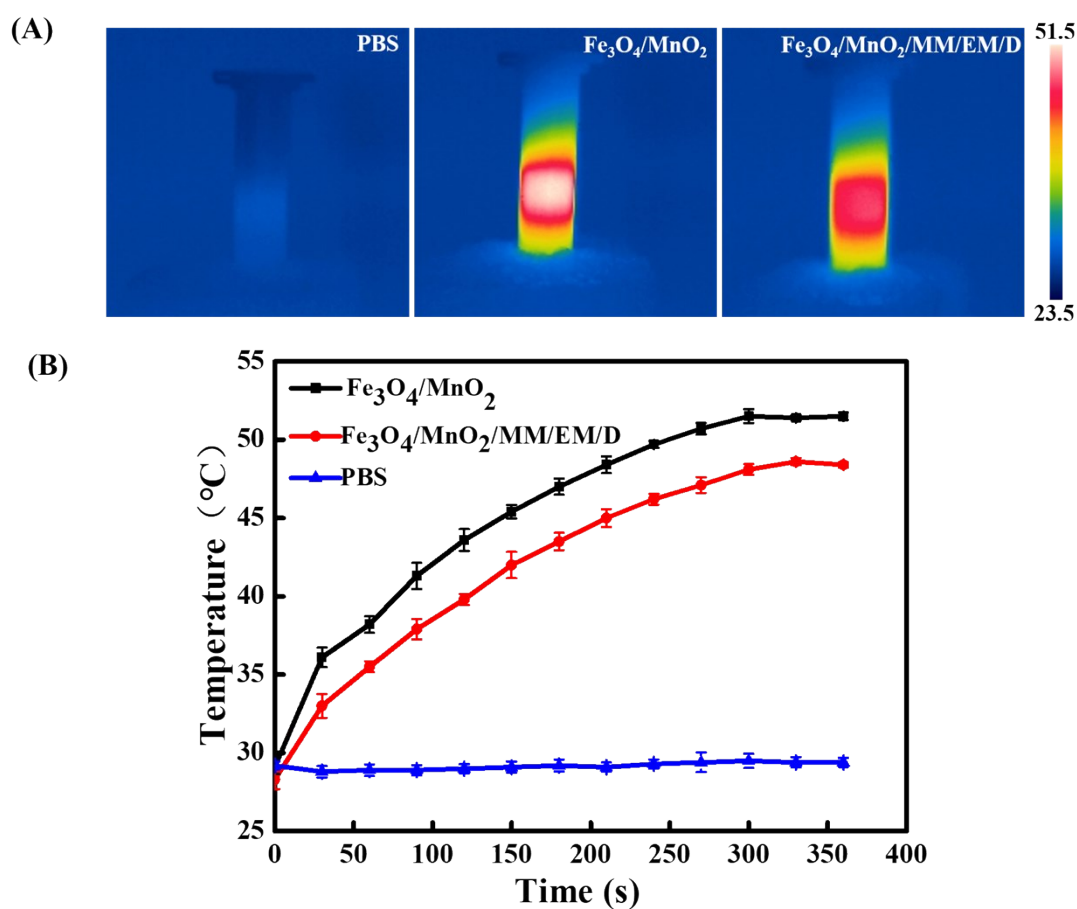


Fig. S6 (A) Infrared thermal-graphic images of PBS, $\text{Fe}_3\text{O}_4/\text{MnO}_2$ and $\text{Fe}_3\text{O}_4/\text{MnO}_2/\text{MM}/\text{EM}/\text{D}$ at 5 min of 808 nm NIR laser irradiation. (B) Temperature elevation curve of PBS, $\text{Fe}_3\text{O}_4/\text{MnO}_2$ and $\text{Fe}_3\text{O}_4/\text{MnO}_2/\text{MM}/\text{EM}/\text{D}$ at 6 min of 808 nm NIR laser irradiation.

In order to explore the cytotoxicity and biosafety of nanoparticles, MCF-7 cells were treated with $\text{Fe}_3\text{O}_4/\text{MnO}_2$ and $\text{Fe}_3\text{O}_4/\text{MnO}_2/\text{MM}/\text{EM}/\text{D}$ at different concentrations (Fe_3O_4 : 50, 30, 20, 10, 5, 2.5 $\mu\text{g}/\text{mL}$) for 24 hours, and the cytotoxicity was evaluated by MTT assay (Fig. S7). In the

cytotoxicity experiment, with the increase of sample concentration, the cell viability of $\text{Fe}_3\text{O}_4/\text{MnO}_2$ nanoparticles did not show obvious changes. After the treatment of 50 $\mu\text{g}/\text{mL}$ $\text{Fe}_3\text{O}_4/\text{MnO}_2$ nanoparticles, the cytotoxicity was not greatly affected, which proved that $\text{Fe}_3\text{O}_4/\text{MnO}_2$ has good biological safety. In particular, the survival rate of $\text{Fe}_3\text{O}_4/\text{MnO}_2/\text{MM}/\text{EM}/\text{D}$ at 50 $\mu\text{g}/\text{mL}$ was only $\sim 33.29\%$, which proved that $\text{Fe}_3\text{O}_4/\text{MnO}_2/\text{MM}/\text{EM}/\text{D}$ was highly toxic to MCF-7 cells.

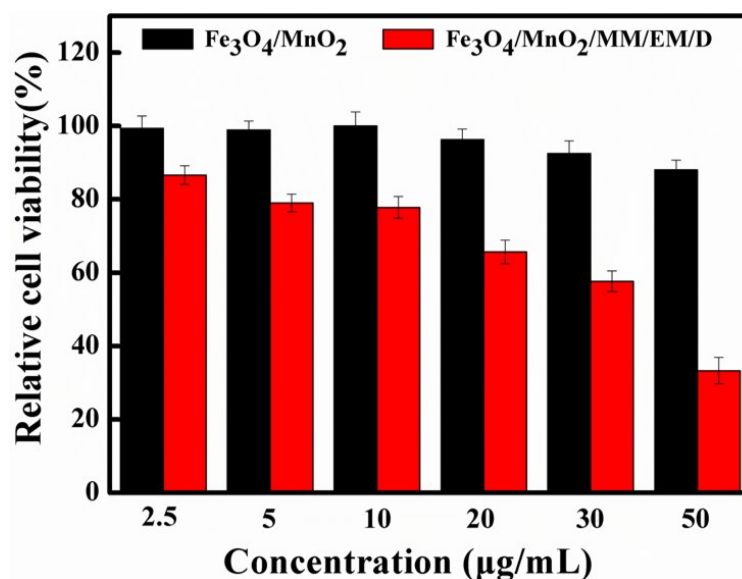


Fig. S7 MTT assays of MCF-7 cells cultured with $\text{Fe}_3\text{O}_4/\text{MnO}_2$ and $\text{Fe}_3\text{O}_4/\text{MnO}_2/\text{MM}/\text{EM}/\text{D}$.

In order to verify the therapeutic effect of $\text{Fe}_3\text{O}_4/\text{MnO}_2/\text{MM}/\text{EM}/\text{D}$ *in vivo*, we established a tumor model by the subcutaneous injection of MCF-7 cells into mice. One week after injection, when the tumor volume of tumor-bearing mice increased to approximately 100-150 mm^3 , the mice were divided into four groups: two of which were injected with PBS, and the other two groups received intravenous injections of $\text{Fe}_3\text{O}_4/\text{MnO}_2/\text{MM}/\text{EM}/\text{D}$ (once every two days). One group of tumor models injected with $\text{Fe}_3\text{O}_4/\text{MnO}_2/\text{MM}/\text{EM}/\text{D}$ and PBS was irradiated with an 808 nm NIR laser with a power density of 3.52 W cm^{-2} for 5 min, and then the temperature of the tumor surface was measured by an infrared camera (Fig. S8A). From the above data, it can be seen that the

temperature of the tumor site of $\text{Fe}_3\text{O}_4/\text{MnO}_2/\text{MM}/\text{EM}/\text{D}$ -treated mice changed significantly after being irradiated by 808 nm NIR laser. After irradiation of 5 min, the local temperature of tumor in mice increased to about "55°C". However, after the same intensity of laser irradiation on 5 min in the PBS-treated group, the local temperature of the tumor area of the mice almost did not change. It is proved that the $\text{Fe}_3\text{O}_4/\text{MnO}_2/\text{MM}/\text{EM}/\text{D}$ injected through tail vein has obvious aggregation in the tumor area, thus achieving a better photothermal conversion efficiency. As shown in Fig. S8B, the temperature of the tumor site of $\text{Fe}_3\text{O}_4/\text{MnO}_2/\text{MM}/\text{EM}/\text{D}$ +NIR-treated mice increased from "35°C" to "55°C" within 5 minutes, which is in line with our expectations of efficient photothermal conversion. To sum up, $\text{Fe}_3\text{O}_4/\text{MnO}_2$ coated by cell membrane has excellent photothermal conversion ability and tumor targeted accumulation potential. It is reported that the heat tolerance of tumor tissue is poor compared with normal tissue.^{6,7} When the local temperature is higher than its heat-resistant temperature, selective necrosis will occur in the tumor tissue. Therefore, the $\text{Fe}_3\text{O}_4/\text{MnO}_2/\text{MM}/\text{EM}/\text{D}$ irradiated by laser may have the ability to induce photothermal ablation of tumor cells, so as to achieve specific targeted therapy of tumor.

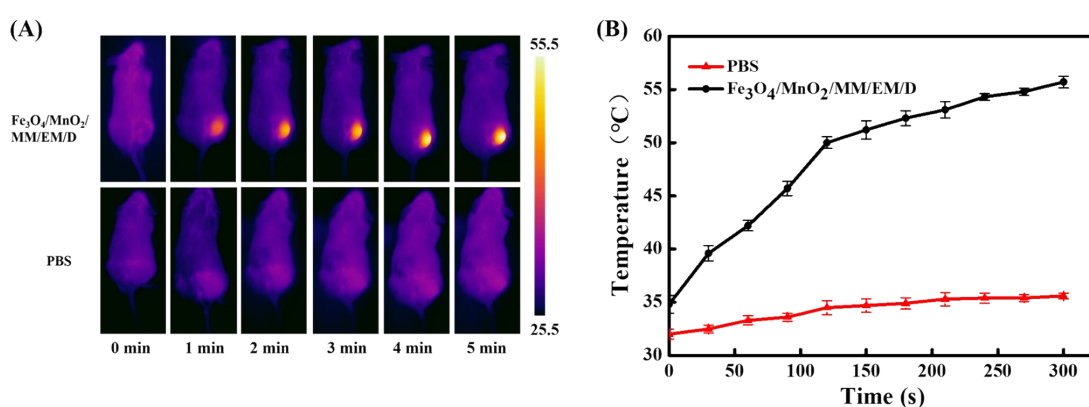


Fig. S8 (A) Infrared thermographic images of MCF-7 tumor-bearing nude mice receiving intravenous injection with PBS and $\text{Fe}_3\text{O}_4/\text{MnO}_2/\text{MM}/\text{EM}/\text{D}$ after 808 nm NIR irradiation. (B)

Temperature increase behaviors of the tumor tissues of MCF-7 tumor-bearing nude mice receiving intravenous injection with PBS and Fe₃O₄/MnO₂/MM/EM/D after 808 nm NIR irradiation.

Based on these results, to evaluate the antitumor effect, the tumor volume of mice was measured every other day after injection. As shown in Fig. S9A, the tumor growth was inhibited in both the Fe₃O₄/MnO₂/MM/EM/D groups and the Fe₃O₄/MnO₂/MM/EM/D +NIR groups, but the tumor volume growth rate in the Fe₃O₄/MnO₂/MM/EM/D +NIR groups were slower than that in the Fe₃O₄/MnO₂/MM/EM/D groups alone. At the same time, the tumor volume of Fe₃O₄/MnO₂/MM/EM treated mice increased more slowly than that of Fe₃O₄/MnO₂/MM treated mice, which indicated that the H₂O₂ produced by the electron transfer reaction of NDH-2 in EM could enhance the therapeutic effect of CDT. By contrast, tumor growth was exuberant in mice treated with PBS. The results showed that the increase in nano-drug accumulation in the tumor greatly improved the therapeutic effect. The change of body weight of all mice were detected as an index of systemic toxicity. It is worth noting that intravenous drug injection and laser irradiation had no significant effect on the body weight of mice (Fig. S9B). These data showed that Fe₃O₄/MnO₂/MM/EM/D has good bio-safety and has almost no effect on normal tissues or organs, so it can be used in the specific treatment of tumors. After 21 days of treatment, all the mice were sacrificed, and the tumors were measured (Fig. S9C). As expected, the tumor volume of mice treated with PBS and PBS+NIR was significantly larger than that of other treatment groups. However, the tumor volume of mice treated with Fe₃O₄/MnO₂/MM/EM/D alone was smaller than that of PBS control groups, and the tumor growth was inhibited to a certain extent. The tumor inhibition effect of mice treated with Fe₃O₄/MnO₂/MM/EM/D+NIR was the most

obvious. The above results showed that CDT/PTT/ chemotherapy can achieve efficient treatment of tumors.

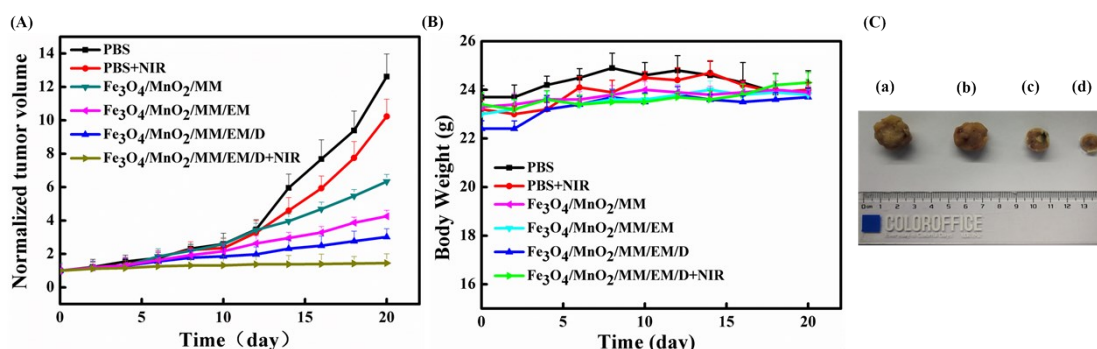


Fig. S9 (A) Normalized tumor volume post-treatment after intravenous injections of various materials. (B) Average body weight of mice after intravenous injections of various materials. (C) Representative digital photographs of the dissected tumors from each group after 21 days treatment. Error bars are based on the standard errors of the mean ($n = 5$).

References

- 1 A. Haque, P. Nandhakumar, G. Kim, S. Park, B. Yu, N. Lee, Y. Yoon, S. Jon and H. Yang, *Anal. Chem.*, 2020, **92**, 3932–3939.
- 2 J. Salewski, A. Batista, F. Sena, D. Millo, I. Zebger, M. Pereira and P. Hildebrandt, *Biochemistry*, 2016, **55**, 2722–2734.
- 3 S. Ahmed, J. Cirone and A. Chen, *ACS Appl. Nano Mater.*, 2019, **2**, 2076–2085.
- 4 L. Gao, J. Zhuang, L. Nie, J. Zhang, Y. Zhang, N. Gu, T. Wang, J. Feng, D. Yang, S. Perrett and X. Yan, *Nat. Nanotechnol.*, 2007, **2**, 577.
- 5 T. Zhang, S. Zhang, J. Liu, J. Li and X. Lu, *Anal. Chem.*, 2020, **92**, 3426–3433.
- 6 A. Jiang, Y. Liu, L. Ma, F. Mao, L. Liu, X. Zhai and J. Zhou, *ACS Appl. Mater. Interfaces*, 2019, **11**, 6820–6828.

7 J. Chen, C. Ning, Z. Zhou, P. Yu, Y. Zhu, G. Tan and C. Mao, *Prog. Mater. Sci.*, 2019, **99**, 1-

26.